WHOI-81-55

THE INFLUENCE OF THE MID-ATLANTIC RIDGE UPON THE CIRCULATION AND THE PROPERTIES OF THE MEDITERRANEAN WATER SOUTHWEST OF THE AZORES

by

Terrence M. Joyce

WOODS HOLE OCEANOGRAPHIC INSTITUTION
Woods Hole, Massachusetts 02543

June 1981

TECHNICAL REPORT

Prepared for the Office of Naval Research under Contract N00014-76-C-0197; NR 083-400, also, partially funded by Study Grant SV-19, NATO.

 In citing this report in a bibliography, the reference given should be to: Journal of Marine Research *39(1): 31-52 (1981).*

Approved for public release; distribution unlimited.

Approved for Distribution: Valentine Worthington, Chairman
Department of Physical Oceanography

Reprint from Journal of Marine Research, Volume 39, 1, 1981.

The influence of the mid-Atlantic Ridge upon the circulation and the properties of the Mediterranean Water southwest of the Azores

by Terrence M. Joyce[1]

ABSTRACT

The warm, salty water influenced by the Mediterranean outflow can be observed at mid-depth throughout the Central North Atlantic Ocean. Katz (1970) first noted that rather than a gradual salinity decrease away from the source, large changes were observable over major topographic features such as the mid-Atlantic Ridge, despite the fact that the topography presented no direct physical barrier to the core layer. Two mechanisms are considered which can account for this sub-surface frontal transition: variable eddy diffusivity and horizontal shear induced by submarine topography. The structure of the actual geostrophic currents and water masses southwest of the Azores is explored with CTD, XBT, and float data collected in June 1977 aboard the R.V. *Knorr*. A CTD section normal to and crossing the ridge axis near 35N, 35W shows the thermocline to be domed up 200 m over the ridge axis compared with stations 200 km to either side. At 1000 meters depth a change in salinity of nearly 0.15‰ in the Mediterranean Water is observed to occur over a horizontal distance of 100-150 km, and is located west of the ridge near 38N and over the ridge axis near 34N. Near this transition two neutrally buoyant floats were tracked for a period of a day. CTD stations around and over a float at 810 meters depth showed the temperature and salinity intrusions to persist with time and horizontal space scales in excess of 15 hours and 4 km. If the currents observed SW of the Azores are representative of the general circulation of the region, they not only explain the water mass structure in the thermocline and Mediterranean Water but also point out that the historical data base of zonal hydrographic sections does not adequately resolve the baroclinic structure.

1. Introduction

The influence of the warm, salty water flowing out of the Mediterrean can be seen throughout the North Atlantic Ocean at depths of 800 to 1500 meters. It was Katz (1970) who first noted that the decrease in salinity westward from Gibraltar was not uniform but discontinuous with rapid changes over topographic features such as the Mid-Atlantic Ridge (MAR) and the Azores-Gibraltar lineament. Katz's rendition of the salinity change along density surface of $\sigma_t = 27.64$ characteristic

1. Woods Hole Oceanographic Institution, Woods Hole, Massachusetts, 02543, U.S.A.

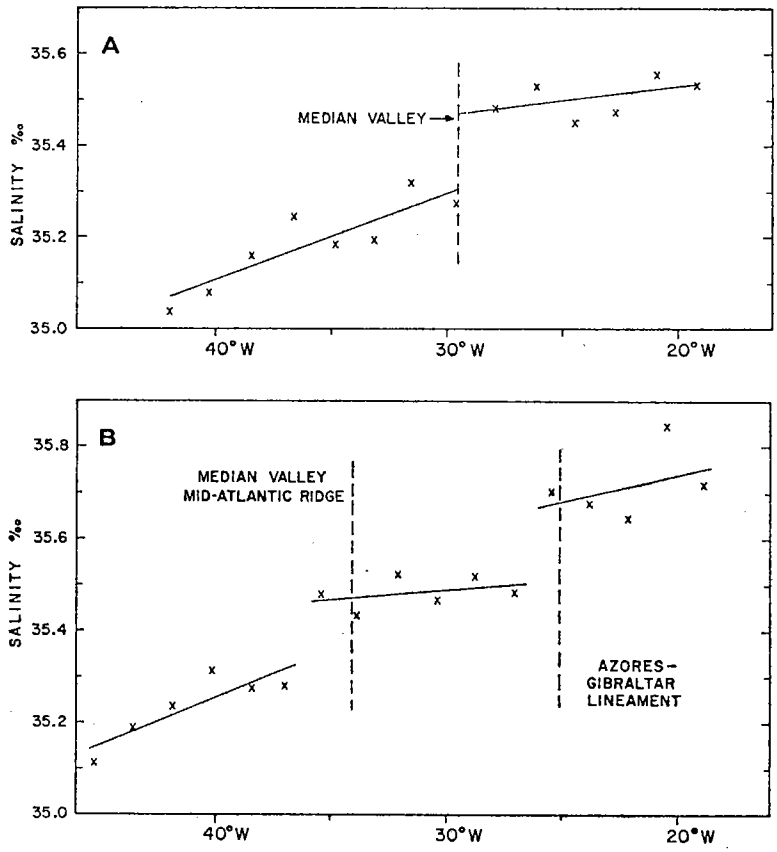

Figure 1. After Katz (1970), the salinity interpolated onto $\sigma_t = 27.64$ from hydrographic sections taken along 40° (upper panel) and 36N.

of the Mediterranean Water core is reproduced in Figure 1 where two east-west sections of IGY data are plotted. On both sections a salinity change of 0.1-0.2‰ occurs in the vicinity of the MAR. He found no evidence that this was happening on the 32N IGY section. It is instructive to plot the core salinity in plan view together with the bottom topography in order to see the extent to which the two may be related. The salinity anomaly data from Needler and Heath (1975) on a potential density surface of 27.7 have been overlaid onto the large-scale bathymetry (after Uchupi, 1971) in Figure 2. Between 34N and 43N the salinity isolines parallel the bottom topography. The overall picture shows a southward slump of the tongue across the North Atlantic with a tendency for the isolines to be closer together on the northern flank than on the southern side. Figure 2 supports the notion that on the northern flank of the tongue, the salinity change is most rapid over topographic features. Contouring much of the same data on the σ_1 surface

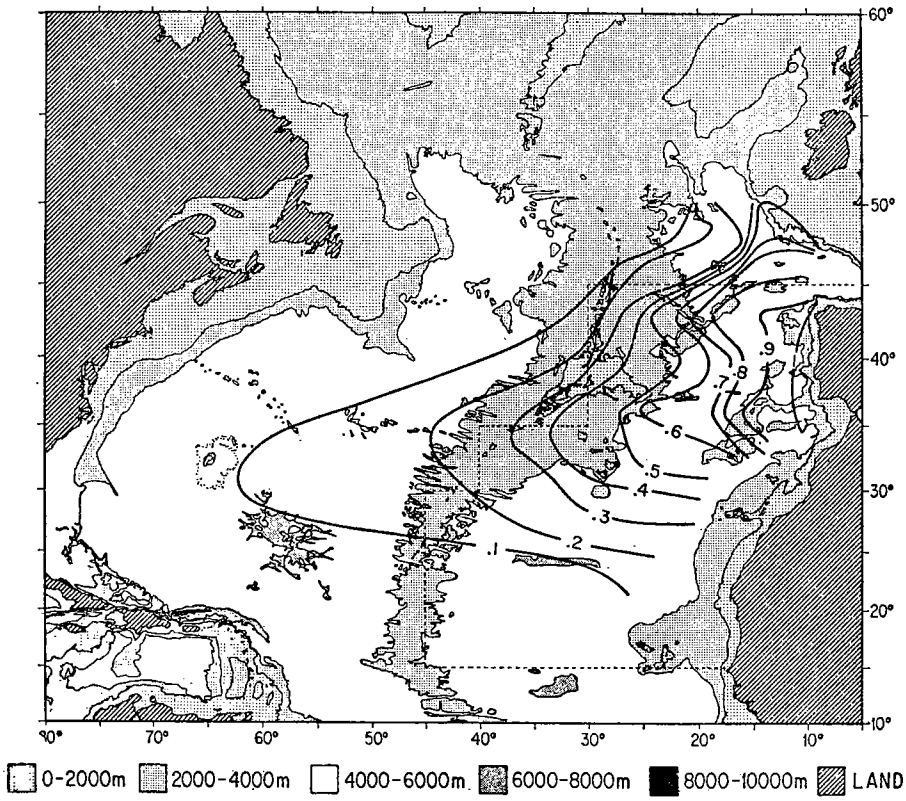

Figure 2. The salinity anomaly relative to 35.01‰ on the potential density surface 27.7 (from Needler and Heath, 1975) overlaid with Uchupi's (1971) topography of the North Atlantic. Dashed line denotes boundary of North African Basin after Wright and Worthington (1970).

32.274 Reid's (1979) salinity map shows many of the features just described. A third piece of evidence for the rapid change in properties of the Mediterranean Water can be found in the volumetric census published by Wright and Worthington (1970). In Figure 3 a portion of the water mass census is reproduced for the North African Basin. Points in the *T/S* diagram containing 50, 75, and 90 percent of the water volume in this basin are coded in the figure. One observes that a low volumetric region or "hole" in the diagram is present for temperatures and salinities between 7-9°C and 35.2-35.4‰. This represents a rapid change in properties of the Mediterranean Water discussed above. Although the warm salty core is shallower than the MAR over most of the North Atlantic, the topography appears to be influencing its properties. In the next section simple steady-state models will be discussed which illuminate mechanisms which can maintain permanent sub-surface fronts (water mass transitions). Following this, new data collected on a section across the MAR southwest of the Azores will be presented showing considerable

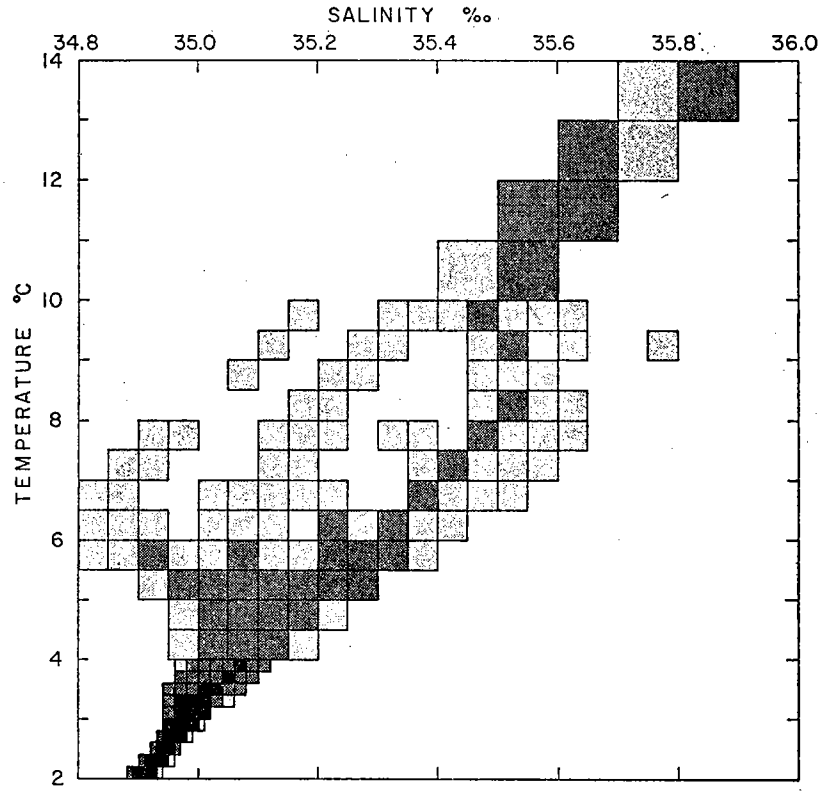

Figure 3. Volumetric *T/S* diagram from Wright and Worthington (1970) for the North African Basin. Black, black + dark grey, black + dark grey + light grey regions contain 50, 75, and 90 percent of water with these *T/S* characteristics within the basin. Below 4°C, potential temperature is used.

structure in the relative geostrophic currents and water masses in this central ocean region.

2. Simple frontogenesis models

The formation of a sub-surface front will be studied considering spatial variations of the: a) lateral mixing, and b) mean currents. In their 3-D advective-diffusive model for the Mediterranean tongue Needler and Heath found vertical mixing to be relatively unimportant in comparison with horizontal terms. Effects of vertical mixing will therefore be neglected for the moment but will be considered later since the two processes are coupled through intrusions within fronts. Within the context of a 2-D advective-diffusive model the governing equation for the longitudinal salinity gradient can be written

$$\frac{d}{dt}\left(\frac{\partial S}{\partial x}\right) = \frac{\partial}{\partial x}\left(\frac{dS}{dt}\right) - \left(\frac{\partial S}{\partial x}\frac{\partial u}{\partial x} + \frac{\partial S}{\partial y}\frac{\partial v}{\partial x}\right), \tag{1}$$

where

$$\frac{dS}{dt} = \nabla_H \cdot (A \nabla_H S) \ . \tag{2}$$

and

$$\frac{\partial}{\partial x}\left(\frac{dS}{dt}\right) = A_{xx}S_x + 2A_xS_{xx} + AS_{xxx} + (AS_y)_{xy} \ . \tag{3}$$

In order to illustrate the two mechanisms for frontogenesis mentioned above, let i) the eddy diffusivity A, the salinity gradient S_x, and the horizontal velocity be independent of y, ii) the salinity gradient S_x have a local maximum, and iii) the currents be steady. For the above example frontogenic processes will tend to increase the perturbation in S_x. For these restrictions (1) becomes

$$\frac{d}{dt}(S_x) = A_{xx}S_x + AS_{xxx} - v_xS_y \ . \tag{4}$$

Irrespective of the sign of S_x, the first term $A_{xx}S_x$ will increase $|S_x|$ if $A_{xx} > 0$. In other words, *fronts will form where there is a local minimum in the diffusivity.* Turner (1973) pointed out in this context that property gradients can be enhanced by variable stirring. The second term in (4) always (for $A > 0$) acts to reduce the magnitude of S_x and need not be considered further. The last term in (4) represents the tendency for horizontal shear to increase concentration gradients. The following example illustrates how the horizontal shear term could be influenced by bottom topography to create a front over a submarine topography.

The linear vorticity balance in a homogeneous, rotating fluid requires in the absence of external forces or dissipation that flow lines will be along contours of constant (f/H), where f is the Coriolis parameter and H is the water depth. Recalling the above restrictions, i)-iii), let a steady uniform current $(U_o,0)$ approach a region of zonally varying depth $H(x)$. Just upstream of a ridge flow will be equatorward with poleward currents on the downstream side. The linear solution is given by

$$\begin{aligned} u &= U_o = \text{const.} \\ v &= +U_o\left(\frac{f}{\beta_H}\right)H_x \ , \qquad \beta \equiv \left(\frac{\partial f}{\partial y}\right) \end{aligned} \tag{5}$$

Substitution of (5) into (4) gives

$$\frac{d}{dt}(S_x) = A_{xx}S_x + AS_{xxx} - \frac{U_o f S_y}{\beta}(\ln H)_{xx} \ . \tag{6}$$

In the northern hemisphere when an eastward current flows north of a tracer core $(S_y < 0)$ a front will form over a submarine ridge crest (where $(\ln H)_{xx} > 0$). The

same obtains for a westward current flowing south of the core. This core is only crudely modeled by a linear change in S with latitude. An actual core has curvature which complicates this discussion by introducing another term (the last one on the right-hand side of (3)) to the balance.

From the above discussion it should be clear that both differential stirring with a local minimum over the ridge crest and horizontal current shear due to bottom topography are candidates for frontogenesis. Neither process is strongly supported in the literature by the existing data.

Dantzler (1977) analyzed North Atlantic XBT data sorted into 2° bins of latitude and longitude and obtained the results shown in Figure 4. The upper panel shows that the 15°C isotherm north of about 34N shoals over the ridge crest with an amplitude of about 50 meters. The modern hydrographic data have been summarized by Stommel, Niiler, and Anati (1978). Though the horizontal resolution is poorer than for the XBT data, the dynamic height between 100 and 1500 decibars shows a doming of about 5 dynamic centimeters in this region over the MAR as with the XBT data. Reid's (1978) analysis of the geopotential anomaly between 1000 and 2000 decibars also suggests a southwest current on the western flank of MAR with an oppositely directed relative current on the eastern side. A CTD section taken normal to the MAR axis southwest of the Azores and presented later again shows this doming with an amplitude about four times greater than the smoothed XBT and hydrographic observations. All of these data lend support to the horizontal current shear mechanism, suggesting a southward deflection of fresh water of western origin along the western side of the mid-Atlantic Ridge enhancing the water mass contrast at the ridge where mixing takes place with the saltier eastern basin Mediterranean Water.

The eddy variability in the North Atlantic at depths of 1000 meters is only beginning to be measured (Schmitz, 1978). No direct measurements for the MAR area have been published but the variability of the 15° isotherm from Dantzler's work might be used to give an indication of eddy activity. The lower panel of Figure 4 shows that most of the variations in eddy potential energy are meridional with little resolvable difference across the MAR. Armi (1979) has argued that such large scale variations translate into important variations in eddy diffusivity. Until some rational scheme is suggested to infer diffusivities at depth from such data, however, the modeling of variable diffusivities must wait.

3. Observations from Knorr Cruise 66, Leg 2

Between 2 and 8 June, 1977, a total of 24 CTD stations were taken southwest of the Azores (Fig. 5), nineteen of which comprise a section across the MAR. The remaining 5 CTD stations were near two neutrally buoyant vertical current meters (VCMs) which were deployed, tracked, and recovered during a one-day period.

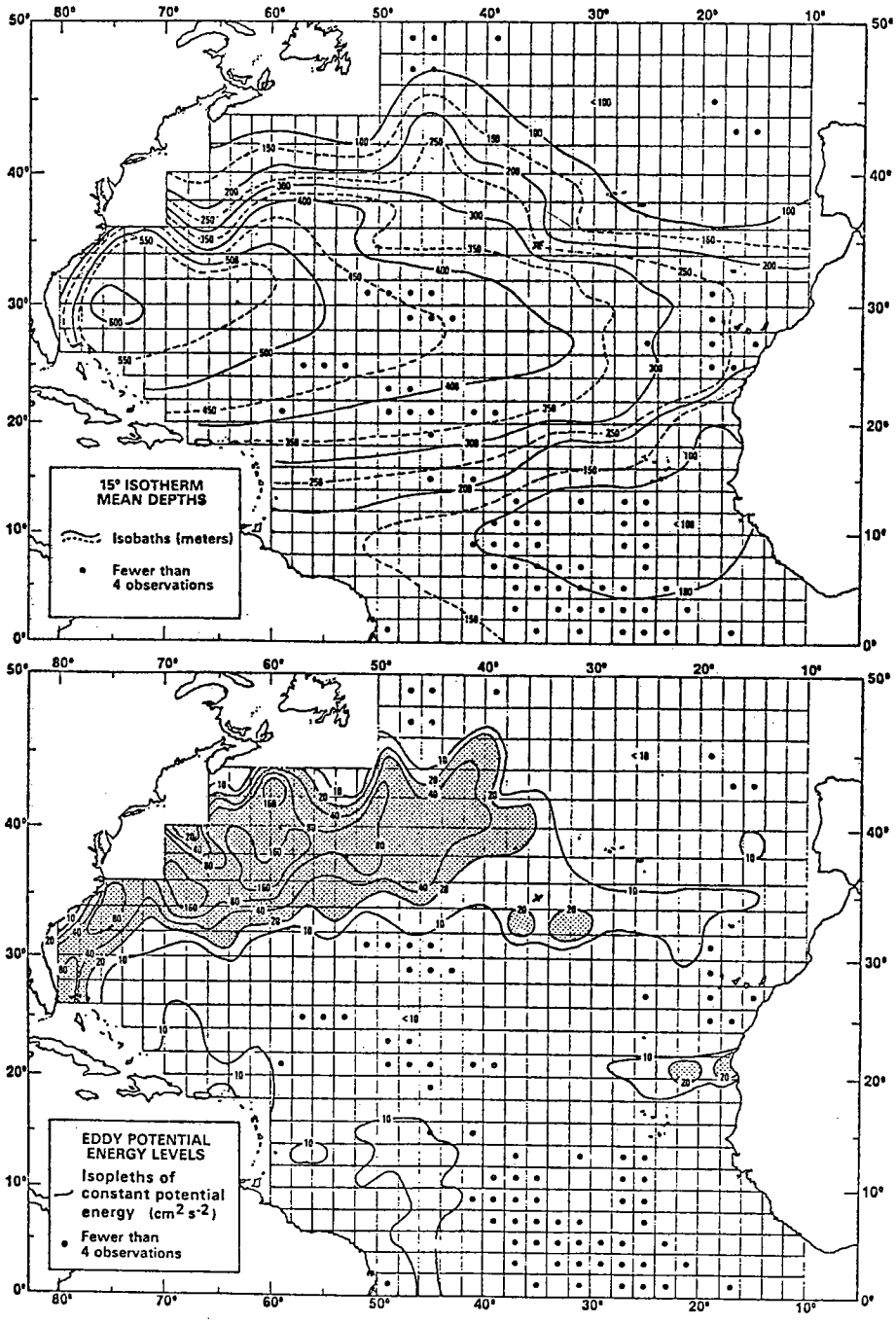

Figure 4. The mean depth of the 15°C isotherm (upper) and the variance multiplied by 1/2 N^2 (lower) from averaged XBT data (Dantzler, 1977).

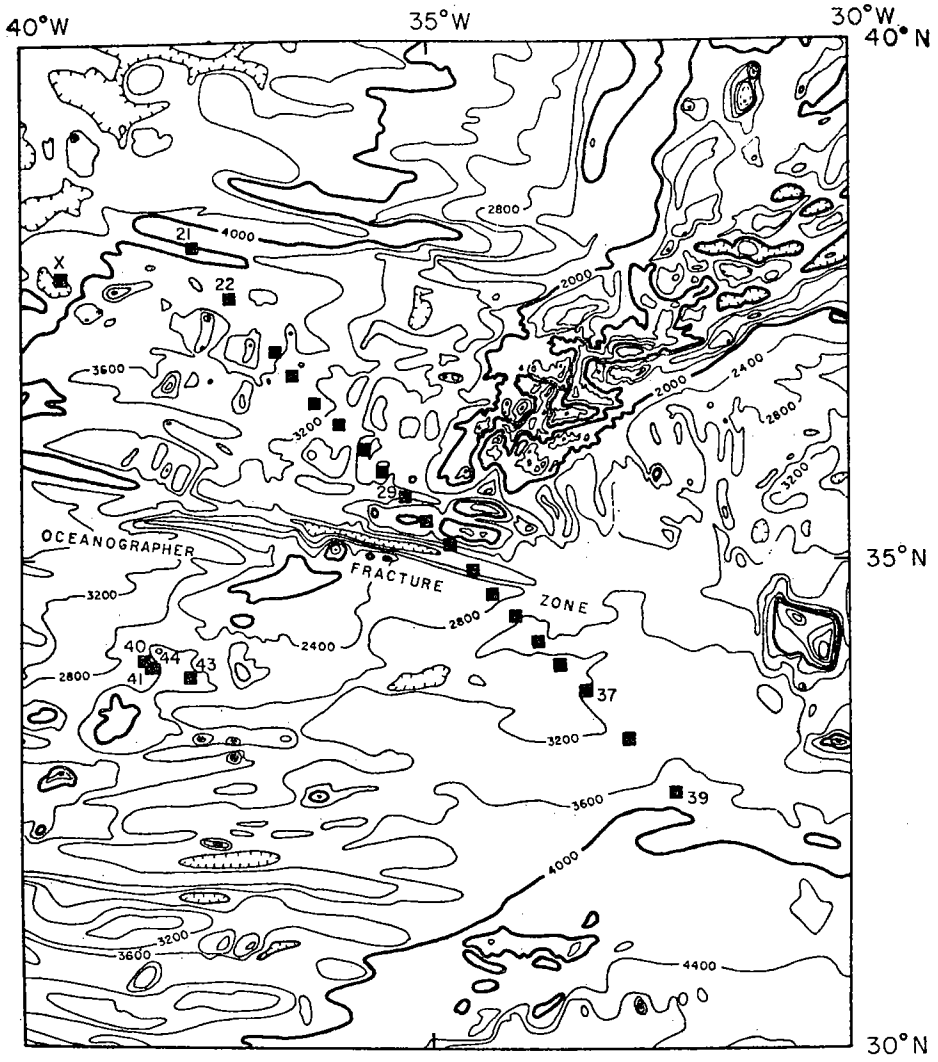

Figure 5. Plan view of CTD stations on *Knorr* 66, leg 2 together with Uchupi's topography in meters. The X in the upper lefthand portion represents the origin of an XBT section (Fig. 8) running through CTD 21 to 39 to 40.

The CTD data were collected with Neil Brown underwater unit equipped with a Beckmann dissolved oxygen probe and a General Oceanics 24-bottle Rosette. Along the section and between CTD stations 39 and 40, T5 XBTs were deployed at roughly 10 n.m. intervals. The deep XBT probes penetrated to 1500 meters through the Mediterranean Water, which was the principle water mass of interest in this study.

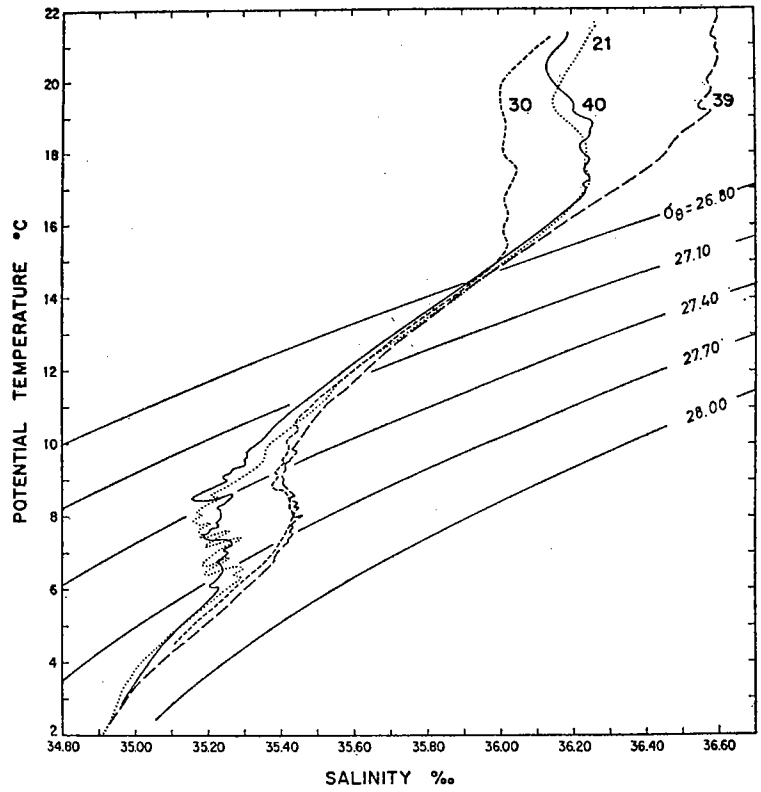

Figure 6. a. Potential temperature versus silinity together with reference lines of constant σ_θ for selected CTD stations.

(a) Water masses. Four CTD stations (21, 30, 39, 40) from the spatial survey have been selected to display the water mass variability in the region. In Figure 6a,b the potential temperature is plotted against salinity and oxygen. The θ/S diagram shows considerable variation in the salinity content of the layer of seasonally warmed water. Against the large-scale trend for sea-surface salinity to increase southwards (c.f., Worthington, 1976), station 21 has near-surface salinities comparable to station 40 which is over 400 km to the south while 30, which also lies south of 21, has the lowest salinity. Both stations 30 and 40 are above the axis of the ridge. The North Atlantic Central Water of the permanent thermocline is uniform in 6a down to depths of the Mediterranean Water where two distinct branches in the θ/S diagram can be seen. Stations 21 and 40 are relatively colder and fresher than 30 and 39 in the density range $\sigma_\theta = 27.2$ to 27.7 gm/liter. Reference to Figure 3 will show this branching to occur precisely at the "hole" in the volumetric T/S diagram. Below this a smooth transition in the deep water takes place going from colder, fresher western basin water to warmer, saltier water of the eastern basin

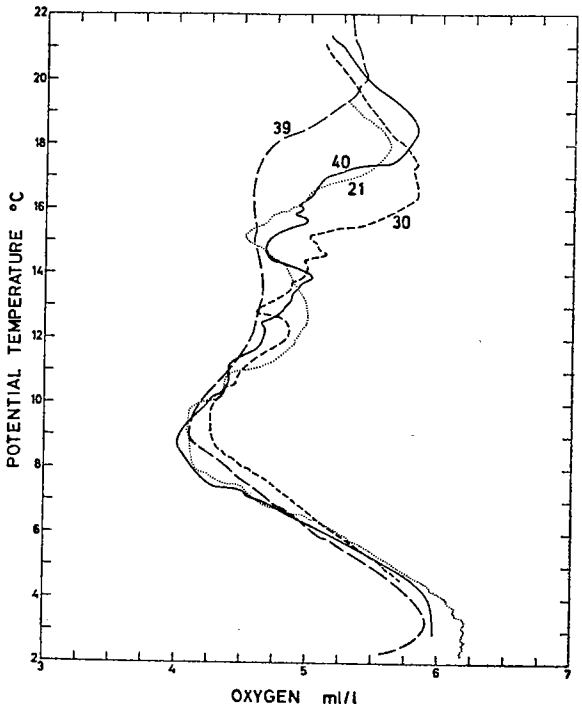

b. Potential temperature versus oxygen for the same stations.

characteristics. At depths below 3000 meters, the MAR represents a physical barrier to exchange between the basins except for isolated passages.

The θ/O_2 diagram (Fig. 6b) shows near-surface maxima of dissolved oxygen at the base of the layer of constant salinity. If one selects temperatures of these maxima and identifies these as remnants of the renewed water from the previous winter, then the wintertime sea surface temperature maps (Böhnecke, 1936) can be used to indicate possible source regions. Stations 30 and 40 over the ridge have temperatures of 17.5 and 18.5 respectively, which correspond to locally found March sea surface temperatures from the monthly mean maps. Stations 21 and 39 have warmer temperatures than the local March means (16.5, 18.5°C respectively) indicating a northeast advection. While the θ/S curves within the permanent thermocline were rather tight, the θ/O_2 diagram shows considerable variability in this domain down to the level of the Mediterranean Water. This can probably be attributed to the influence of recently renewed water of more northwesterly origin upon the waters of the thermocline. The oxygen minimum layer at $\theta \sim 9$°C shows some oxygen variability but no coherent pattern over the region. This will be more apparent later in the O_2 section across the ridge. The deep water shows considerable change in oxygen with higher values on the western side of the MAR.

(b) CTD section. Stations 21-39 comprise a section across the axis of the MAR and will be presented as a hydrographic section with the observed pressure of a particular isoline of temperature (7a), salinity (7b), dissolved oxygen (7c), and potential density (7d) displayed together with the local bottom pressure. Due to propeller noise, no bottom echoes could be obtained while the ship was underway at normal speed (10 knots). The bottom returns plotted are those when the ship slowed for XBTs or stopped for a CTD station. Reference to Figure 5 should convince the reader that the topography is complicated in the region. A peak in the section could be entirely absent 10 n.m. normal to the plane of the bottom profile. For this reason the isolines have not been forced to be normal to the bottom as is often done with sections. Concluding the presentation of the CTD section, a calculation of geostrophic velocities relative to the deepest common level and 1500 dbars has been made and plotted as Figures 7e,f. Above the figures are shown the CTD station numbers with tic marks denoting XBT positions and bathymetric readings. The distance between these tic marks is nominally 10 n.m.

Figure 7a shows the doming of the temperature isolines in the upper 1000 meters over the MAR which was anticipated from the mean XBT pattern (Fig. 4). In particular the 15°C isotherm rises 200 decibars between stations 24 and 30 and thereafter drops 300 decibars (dbars). Little relief is evident in the temperature field below 2000 dbars although this will be apparent in the density isolines. The doming of the Central Water over the axis of the ridge brings fresher thermocline water nearer the surface over the ridge axis than to either side. This could locally influence the depth and salinity of the convectively formed winter water, would explain the low near surface salinities of the stations (e.g., 30, 40) over the ridge axis, and is consistent with oxygen data which suggests in the θ/O_2 diagram a local origin for this water. Below 1500 dbar a gradual downward slope to the salinity isolines from left to right is observed as the deep water becomes gradually saltier at a given pressure toward the southeast. The Mediterranean Water level is centered at 1000 dbar and is marked by numerous inversions and blobs in the salinity section; no attempt has been made to join these together. Although a change in the salinity of the core is observed over the ridge crest, the principle change occurs between stations 21 and 22 at the extreme NW end. This change will be discussed in detail later. The oxygen minimum layer continues in somewhat broken fashion across the section with no major trend. The deep water to the northwest is higher in dissolved oxygen as is the water of the thermocline. The 5 ml/l isoline rises up nearly 300 dbars between stations 22 and 30 at the ridge crest. Thermocline waters have higher oxygen, in general, on the western flank of the ridge axis than on the eastern side. There is considerable vertical structure to the oxygen profiles in the thermocline and it appears to be a particularly interesting tracer at these depths much like the salinity in the deeper Mediterranean Water layer. The predominant feature of the density section (Fig. 7d) is a doming of the isopycnals over

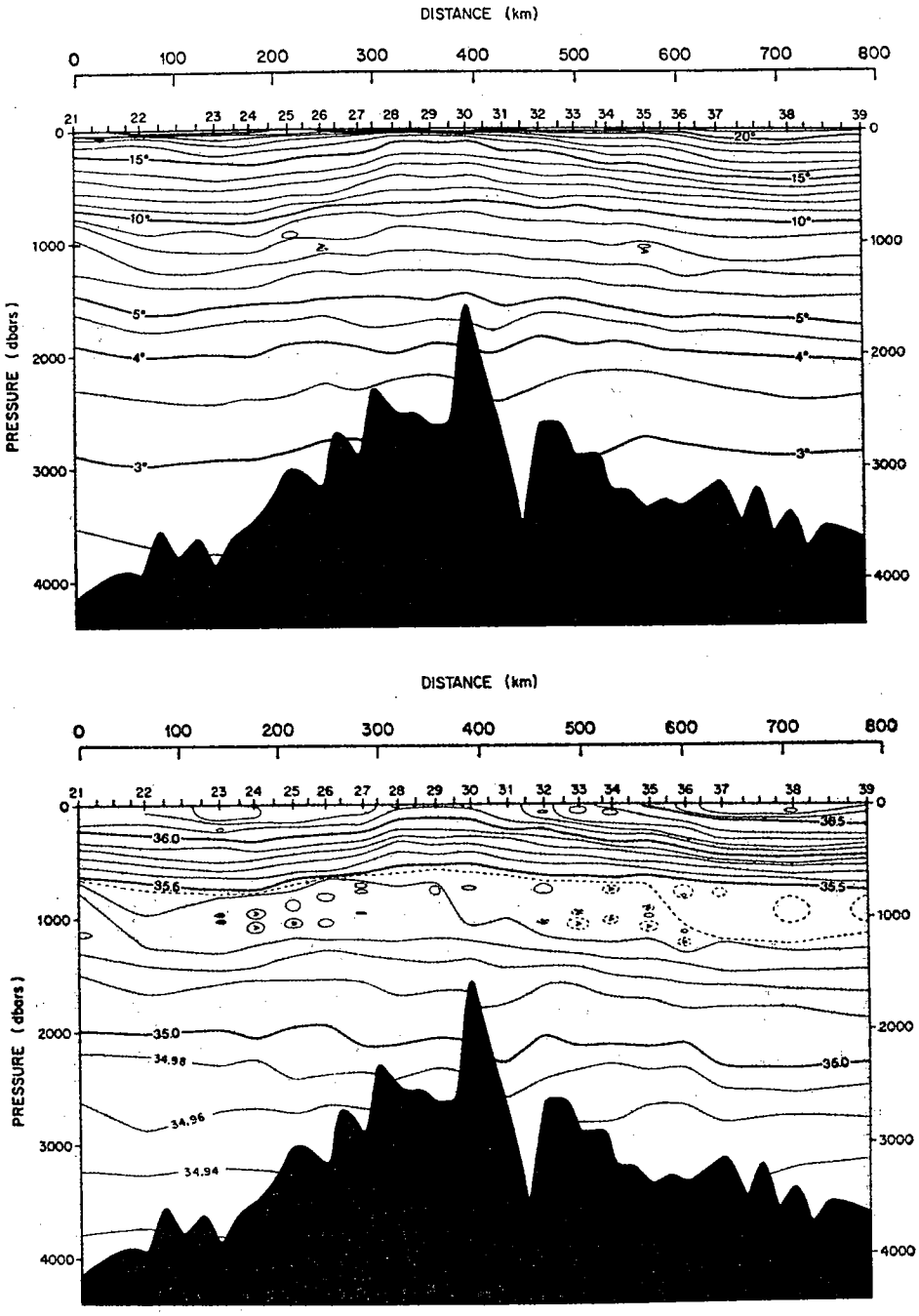

Figure 7. a. Temperature section across ridge axis showing isotherm and bottom topography versus pressure. Average spacing between stations over ridge axis is 36 km for a total section distance of about 790 km.

b. Salinity section. Dashed line indicates 35.45‰ isoline. Positive inversions labeled, otherwise "less than" is understood.

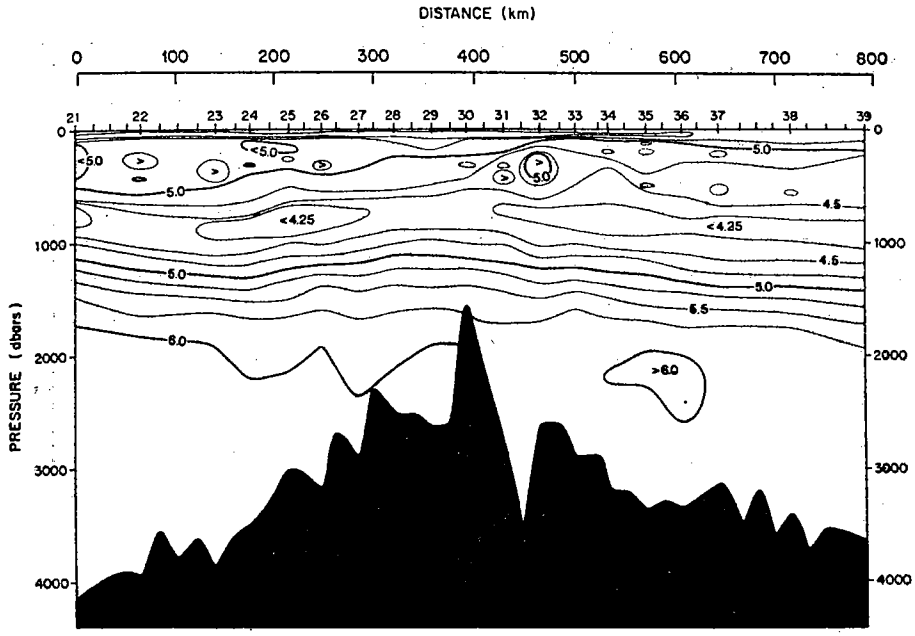

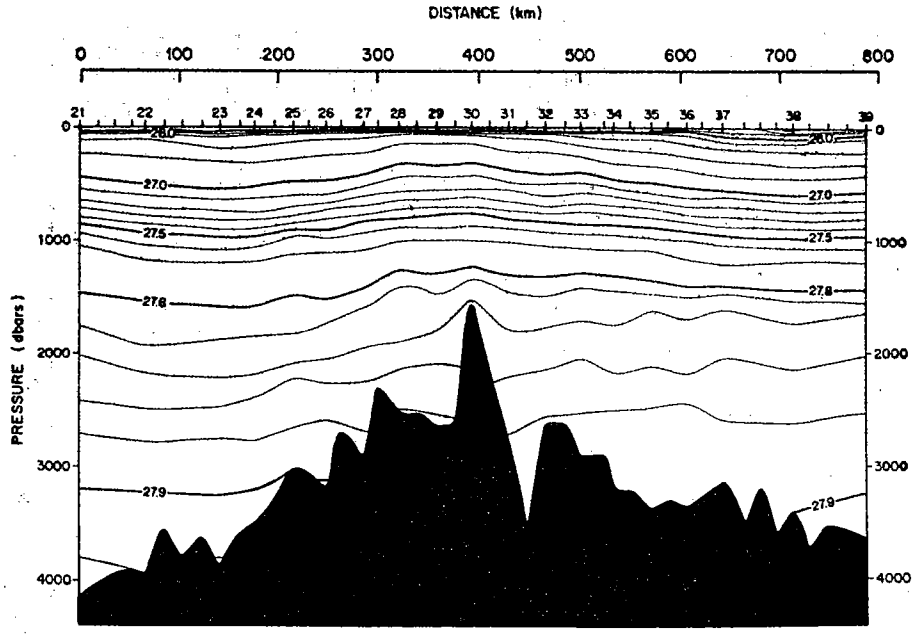

c. Same as 7a but for dissolved oxygen in m*l*/*l*.

d. Same as 7a but for potential density.

the MAR axis. The density line $\sigma_\theta = 27.7$ used by Needler and Heath, denoting the core of the salinity anomaly in Figure 2, is elevated 200 dbars in station 30 compared to stations 23 and 37 which are 200 km to either side.

The effect of the isopycnal doming is certainly reflected in the following figure (7e) of the geostrophic currents relative to the deepest common level between adjacent stations. The baroclinic volume transports between stations 21, 23, 30, and 38 are +17, −31, and +27 $\times$ $10^6 m^3 sec^{-1}$ respectively. At depths of the Mediterranean water relative geostrophic currents of 5-10 cm sec^{-1} are calculated changing sign over the axis of the MAR. On the northwest side of the section a current reversal is observed.

According to Worthington's (1976) deep circulation scheme, a southward flow of water with temperatures between 2°C and 4°C is required west of the MAR at a latitude of 38N, near the NW end of the CTD section. If deep velocities are to be anticipated then a choice of a bottom reference surface is inappropriate. In 7f a 1500 dbar reference surface is used which allows for weak southeast flow between stations 21 and 23 but also shows a stronger component in the opposite direction centered between stations 24 and 25. In order to minimize the number of flow reversals on the western side of the MAR, the reference surface must be allowed to slope. The nearest deep current observations on the western flank of the MAR are at 27N (Fu and Wunsch, 1979, POLYMODE News #60) far south of this section and the latitude where Worthington indicates a strong, deep flow.

The water masses and geostrophic velocities in the eastern basin are considerably less complicated in the CTD section: the general trend suggests a northeasterly flow component at most depths. This was in fact anticipated in some of the earlier hydrographic data summaries already discussed. The nearest moored current observations in the eastern basin come from a 15-day time series at 29N, 29W near Meteor Seamount by Horn, Hussels, and Meinke (1971) in which the 15-day mean current at 1200 meters was 2 cm sec^{-1} northwards. The series is rather short, however, and the flow likely to be influenced by the proximity to the seamount. A hydrographic section across the eastern basin north of the Azores by Swallow, Gould, and Saunders (1977) shows significant northward flow only near the continental boundary. There is only a weak suggestion for the doming of the thermocline over the ridge axis (P. Saunders, personal commun.).

(c) XBT sections. Before, during, and after the CTD section above, XBTs were taken; these results will now be discussed. Reference to Figure 5, the plan view of the stations, shows west of CTD 21 an X which denotes the origin of an XBT section which runs from northwest to southeast crossing the ridge axis near CTD 30 and continuing to CTD 39 where the section turns back westward proceeding to CTD 40. A combination of either temperature or fall rate errors in the XBTs prevents a merger of the CTD and XBT measurements. A preliminary report of the